

# Nonlinear lattice model of viscoelastic Mode III fracture

David A. Kessler\*

*Dept. of Physics, Bar-Ilan University, Ramat-Gan ISRAEL*

Herbert Levine†

*Dept. of Physics, Univ. of Cal., San Diego, La Jolla, CA 92093-0319 USA*

We study the effect of general nonlinear force laws in viscoelastic lattice models of fracture, focusing on the existence and stability of steady-state Mode III cracks. We show that the hysteretic behavior at small driving is very sensitive to the smoothness of the force law. At large driving, we find a Hopf bifurcation to a straight crack whose velocity is periodic in time. The frequency of the unstable bifurcating mode depends on the smoothness of the potential, but is very close to an exact period-doubling instability. Slightly above the onset of the instability, the system settles into an exactly period-doubled state, presumably connected to the aforementioned bifurcation structure. We explicitly solve for this new state and map out its velocity-driving relation.

## I. INTRODUCTION

The problem of dynamic fracture has received increasing attention in the physics community in the last decade [1]. The experiments of Fineberg, et. al. [2], showing interesting dynamical behavior for large velocity cracks have been at the center of this growing interest. From a theoretical point of view, the singularities at the crack tip associated with continuum treatments of the crack problem make the problem challenging. The presence of these singularities necessitates a treatment of the crack at the microscopic level, where the continuum treatment and its associated singularities are not applicable. One line of attack on this problem, initiated by Slepyan [3], has been through the study of lattice models of cracks. These lattice models are simpler than full atomistic simulations [4] in that the connectivity of the atoms is specified from the beginning, and so dislocations are excluded.

Much progress has been made in understanding steady-state propagation of cracks in lattice systems [3, 5, 6, 7, 8]. A key simplifying assumption underlying much of this progress has been the assumption of piecewise-linear forces between the particles, so that the particles interact with Hookean springs, which break at some critical extension, reducing the force to zero. With these piecewise-linear interactions, the model admits an analytic solution via the Wiener-Hopf technique. This solution has been carried out both for Mode I and Mode III cracks, for both finite width and infinitely wide systems, with and without dissipation.

A general feature of these solutions is that they are problematic at both very small and very large (roughly above 0.7 of the wave speed) velocities. For small dissipation, the solutions are inconsistent at small velocities, in that bonds on the crack surface which are assumed to crack at time  $t = 0$ , say, in fact are seen to crack earlier. For large dissipation, the small velocity solutions are consistent, but exhibit a backward (velocity increasing with decreasing driving) velocity/driving curve, indicating the solutions are unstable. Thus, in any case, stable solutions are not found for small velocities.

At large velocities, the analytic solutions are again inconsistent, this time due to the breaking of additional bonds not on the crack surface. The analytic methods thus are unable to tell us anything about the dynamics beyond this point.

An additional limitation of the piecewise-linear force law is that it complicates the task of constructing a linear stability treatment of the steady-state crack. This is due of course to the discontinuous nature of the force law. For these reasons, we choose in this paper to examine steady-state crack propagation in lattice models with arbitrary force-laws. In particular, we study a family of force-laws parameterized by  $\alpha$ , such that for small  $\alpha$  the force-law is smooth and the force-law goes over to the piecewise-linear one in the limit of infinite  $\alpha$ . We have previously studied [9] the behavior of arrested Mode III cracks with this family of force-laws, and found that the range of drivings for which arrested cracks exists narrows sharply as  $\alpha$  is reduced from infinity. In this paper we examine moving Mode III cracks for varying  $\alpha$ . We find that the behaviour for small velocity is very sensitive to  $\alpha$ . For large velocities, we find that the effect of finite  $\alpha$  is to convert the inconsistency to a regular linear instability, here of Hopf type. We show that

---

\*Electronic address: kessler@dave.ph.biu.ac.il

†Electronic address: levine@herbie.ucsd.edu

at some distance into the unstable regime, the system adopts a new form of steady-state behavior which breaks the symmetry across the crack surface and has a period-2 structure. We conclude with some observations about the model deep in the unstable regime.

## II. MODEL AND GENERAL METHODOLOGY

In this paper, we study a triangular lattice model of Mode III cracking. We take the force exerted at site  $\vec{x}_1$  by the displacement at nearest neighbor site  $\vec{x}_2$ , with (scalar) displacements  $u_1, u_2$ , respectively to be

$$f_{1,2} = (u_2 - u_1) \frac{1 + \tanh(\alpha(1 - \sigma_{1,2}(u_2 - u_1)))}{1 + \tanh(\alpha)} \quad (1)$$

where  $\alpha$  is a parameter which controls the smoothness of the potential and  $\sigma$  is positive if  $\vec{x}_2$  lies to the left of  $\vec{x}_1$  or is further from the crack plane  $y = 0$ . This form has the feature that the force goes to zero at large positive extensions of the nearest-neighbor springs. In the limit of large  $\alpha$ , this force-law approaches a step-function, (with critical spring extension 1), a form introduced by Slepyan[3], and the subject of much investigation[5, 6, 7, 8, 10, 11]. The lattice has  $2N + 2$  rows in the  $y$ -direction, separated by a distance  $\sqrt{3}/2$ , so that the rows are labeled from  $y = -(2N + 1)\sqrt{3}/4$  to  $y = (2N + 1)\sqrt{3}/4$ . The displacements  $u$  of the bottom and top rows at  $y = \pm(2N + 1)\sqrt{3}/4$  are constrained to be  $\pm\Delta$ . We introduce a Kelvin-type viscosity parameterized by  $\eta$  via an additional dissipative force

$$g_{1,2} = \eta k_{1,2} \frac{d}{dt}(u_2 - u_1) \quad (2)$$

where  $k_{1,2}$  is an effective spring constant

$$k_{1,2} = f_{1,2}/(u_2 - u_1) \quad (3)$$

This form was chosen so as to ensure a purely dissipative force which in the limit of large  $\alpha$  goes over to the form  $\eta\theta(1 - (u_2 - u_1))(\dot{u}_2 - \dot{u}_1)$  studied in connection with dissipation in the piecewise-linear model [6, 7, 8, 12].

These forces define the model. The equation of motion is simply

$$\ddot{u}_{\vec{x}} = \sum_{\vec{x}' \in nn} (f_{\vec{x},\vec{x}'} + g_{\vec{x},\vec{x}'} ) \quad (4)$$

We shall primarily be interested here in steady-state cracks, where the displacements have the Slepyan form  $u_{x,y}(t) = u_y(t - x/v)$ . Furthermore, we will focus on symmetric cracks, such that  $u_{-y}(t) = -u_y(t + 1/(2v))$ , which is the symmetry appropriate to steady-state cracks in the piecewise-linear model [5]. Then, solving for the steady-state crack means solving for  $N$  functions of time, characterizing the time development of a typical mass point in each row of the lattice. The equations are non-local in time, due to the coupling between different lattice points. As there is no hope of constructing analytic solutions at general  $\alpha$ , we solve this problem numerically.

To proceed, we discretize the time variable in units of some small  $dt$ . The key insight involved in constructing a numerical procedure is noting that the steady-state equations have a banded structure, just as was the case for the piecewise-linear model [6]. This is due to the fact that mass points are coupled to nearest neighbors, which gives rise via the Slepyan ansatz to a coupling to displacements at a finite time separation. Of course, the equations here are everywhere nonlinear and we need to employ Newton's method to find a solution. This is nonetheless computationally feasible, since the update step in Newton's method is a linear problem with the aforementioned banded structure.

Imagine searching for a solution assumed to have some velocity  $v$ . There is one equation of motion for each displacement field  $u_y$  at each discrete instant in time. In addition, fixing the translation invariance by some condition such as  $u_{\sqrt{3}/4}(0) = 1/2$  gives one additional equation, which we can use to solve for the driving displacement  $\Delta$ . The only problem is that  $\Delta$  is involved in many different equations and so destroys the banded structure of the problem. Two different ways to circumvent this difficulty present themselves. The simpler of the two is to guess, for a given velocity, a value of  $\Delta$ , and solve a modified system of equations where the equation of motion at  $t = 0, y = \sqrt{3}/4$  has been dropped, and the time translation has been fixed. The resulting banded problem can be solved economically, and the violation of the dropped equation of motion calculated. This defines a mismatch function, which has a zero at the true value of  $\Delta$ , which is located by a standard zero-finding routine. A more efficient approach is to realize that solving the entire linear system can be accomplished at essentially no more expense than the fully banded modified system of the first approach. The algorithm for achieving this is presented in Appendix A. The advantage of this approach is that the Newton solver produces a value of  $\Delta$  directly, without the need of invoking a outer root-finding routine.

### III. THE SMALL VELOCITY REGIME

We have already seen in [9] that smoothing the form of the force-law effects a dramatic reduction in the window of drivings for which arrested cracks exist. As the moving crack solution arises as a backward bifurcation of the arrested crack, we can expect that small velocity cracks are also extremely sensitive to the smoothness of the force-law. An indication of this can be found in our previous study [6, 7] of a continuous- $x$ , discrete- $y$  model, which did not have any window of arrested cracks. There the velocity rose linearly from zero as the driving  $\Delta$  increased from the Griffith value  $\Delta_G$ , with a slope inversely proportional to  $\eta$ . The study of small velocity solutions with sharp but not discontinuous force laws should be directly related to experimental data on the onset of propagating cracks in materials such as single crystal silicon [13].

As mentioned above, we solve the steady-state problem via Newton's method. We present in Fig. 1(a-c) a graph of  $v$  versus  $\Delta/\Delta_G$  for various values of  $\eta$  and  $\alpha$ , together with the results from the piecewise-linear limit. We chose to

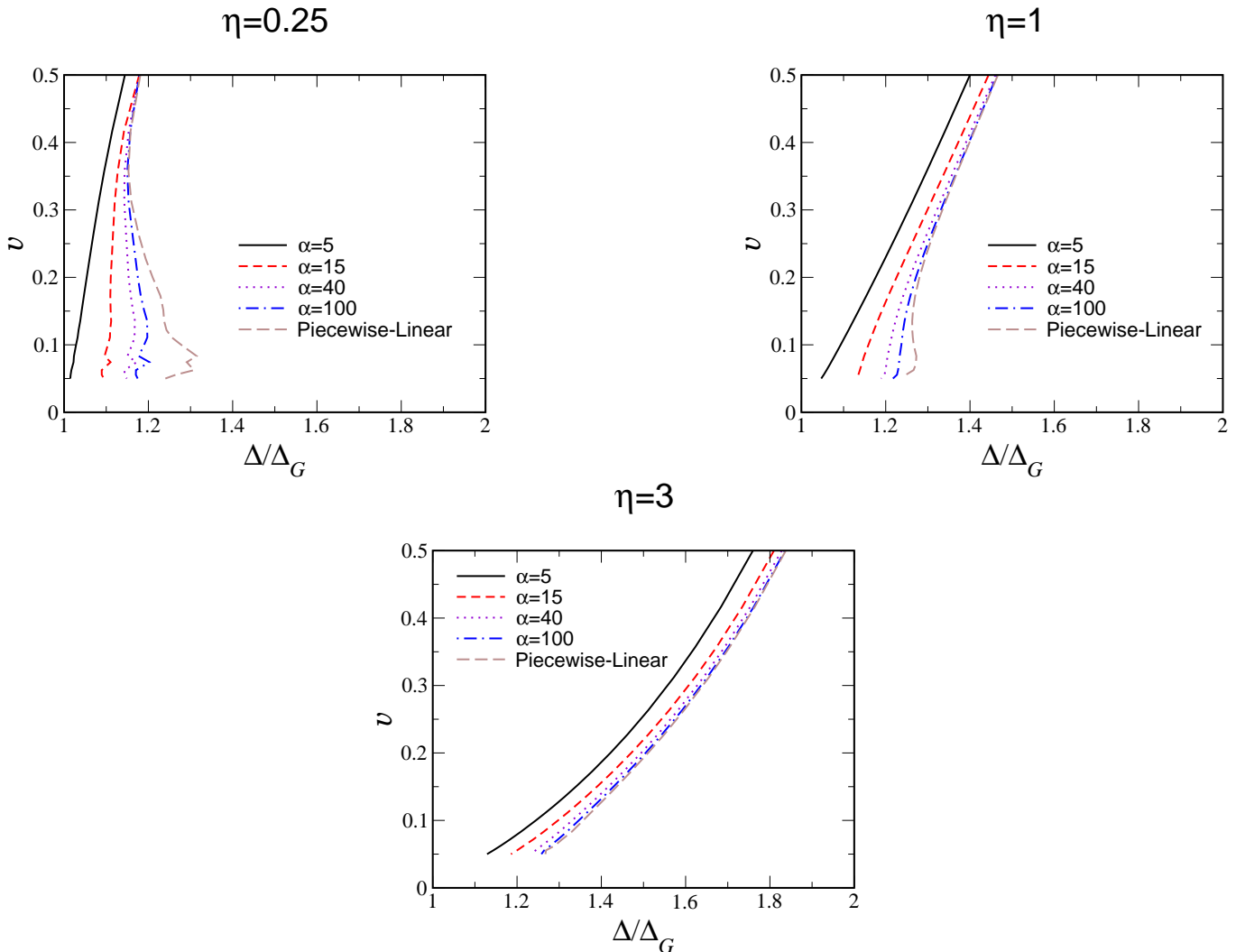


FIG. 1: Dependence of  $v$  on  $\Delta/\Delta_G$  for  $\alpha = 5, 15, 40$ , and  $100$  together with the piecewise-linear model for  $\eta = 0.25, 1$  and  $3$ .  $N = 3$ ,  $dt = 0.1$ .

present data for  $N = 3$  so as to be able to investigate smaller velocities at reasonable computational cost; the small velocity regime is relatively insensitive to  $N$  [6]. A few general trends are evident from these plots. First, the effect of  $\alpha$  is much more pronounced at small velocity. Second, smoothing the potential by decreasing  $\alpha$  postpones the onset of the backward branch of the curve to lower velocity. This is consistent with the narrowing of the window of arrested cracks with decreasing  $\alpha$ , since the curve is forced to turn back to meet the end of the arrested crack branch. Decreasing  $\alpha$  also decreases the amplitude of the oscillations present at small  $\eta$ . Examining the effect of varying  $\eta$ , we see that the larger  $\eta$ 's are less sensitive to  $\alpha$ . This is to be expected, since even in the piecewise-linear model  $\eta$  reduces

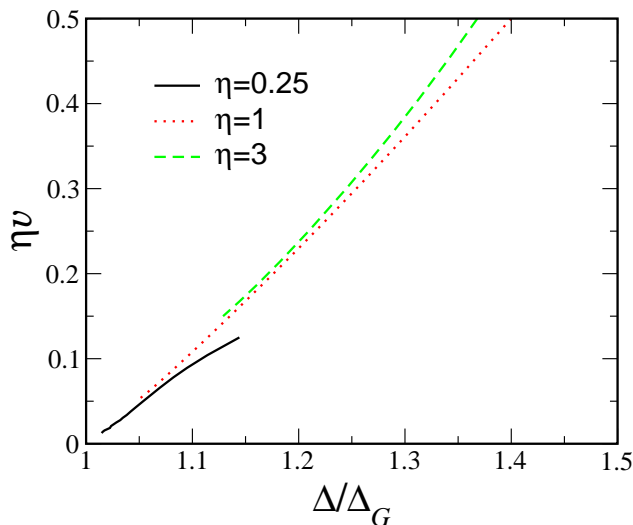


FIG. 2: Dependence of  $\eta v$  on  $\Delta/\Delta_G$  for  $\alpha = 5$ , for  $\eta = 0.25, 1$ , and  $3$ . Again,  $N = 3$ ,  $dt = 0.1$ .

the extent of the backward branch which is one of the primary consequences of having smaller  $\alpha$ . This reduction is related to the increase in the size of the process zone with increasing  $\eta$  [7], which smoothes out the lattice structure in a similar manner to that accomplished by smoothing the potential. Thus, in general, decreasing  $\alpha$  and increasing  $\eta$  both act to reduce the lattice-trapping effects which give rise to the backward branch. It should be noted that this analysis is consistent with the onset of running cracks directly above  $\Delta_G$  in a molecular dynamics simulation using Lenard-Jones potentials[14].

Another way to see that reasonably smooth force-laws give rise to essentially  $x$ -continuum behavior is to look at  $\eta v$  as a function of  $\Delta$  for different  $\eta$ 's. In Fig. 2, we present the data for the case  $\alpha = 5$ . We see that the data overlap extremely well, except for the highest velocity data for each value of  $\eta$ . This is an indication that, as in the  $x$ -continuum problem [6], the only velocity scales are  $\eta$  and the wave speed,  $c = \sqrt{3/2}$ . For the piecewise-linear model, on the other hand, where the  $x$ -lattice scale is important, the  $\eta v$  scaling [15] only sets in for large  $\eta$ , where the process zone is large [7].

The other point of interest is the nature of the solutions for small  $\eta$ . In the piecewise-linear model, the solutions on the backward branch are inconsistent at small  $\eta$ , since the underdamping of the forward running waves leads to pre-cracking. This is of course not a problem in our fully nonlinear model, since cracking here is a reversible process. Nevertheless, it is amusing to note that the solutions on the backward branch for small  $\eta$  do not behave in this manner. They do not crack and reheal. Rather, they exploit the smooth transition in the force law to crack in a slow, monotonic fashion. We show in Fig. 3a the extension of the bond along the crack surface as a function of time, for  $\alpha = 40, 100$ , and  $200$ , along with the analogous result for the piecewise-linear model. We see that the limit of large  $\alpha$  does not correspond to the behavior of the piecewise-linear model. Not surprisingly, then, it turns out the  $v$  vs.  $\Delta$  curve for large  $\alpha$  does not converge to the piecewise-linear result. Thus, for example, for the case considered in Fig. 3a, namely  $N=3$ ,  $v = .1$ ,  $\eta = 0.25$ , the limiting value of  $\Delta/\Delta_G$  for large  $\alpha$  is  $1.2140$ , as compared to  $1.2778$  for the piecewise-linear model. Whereas the bond extension surpasses the critical extension of unity in the piecewise-linear model, and then returns to unity before cracking, the bond extension in the nonlinear model is monotonic, and spends a long time near critical extension. A clearer picture of this emerges in Fig. 3b, where we present the force exerted by the bond as a function of time for the nonlinear model. We see that the bond exploits the nonlinearity of the force-law to crack in a very slow fashion.

#### IV. THE LARGE VELOCITY REGIME

It is known [5, 11] that the piecewise-linear solution is inconsistent at large velocity due to the cracking of other bonds. This has been extensively studied for the Mode III problem in an infinite square lattice and well as for Mode I in a triangular lattice[8]. We thus expect that for velocities larger than the critical one at which the inconsistency first appears, the solutions of our nonlinear model will diverge significantly from those of the piecewise-linear model.

To begin, we use our steady-state code to find large velocity solutions of the equations of motion. We present in Fig. 4 data for  $v$  versus  $\Delta/\Delta_G$  at three values of  $\alpha$ , together with the analogous results from the piecewise-linear

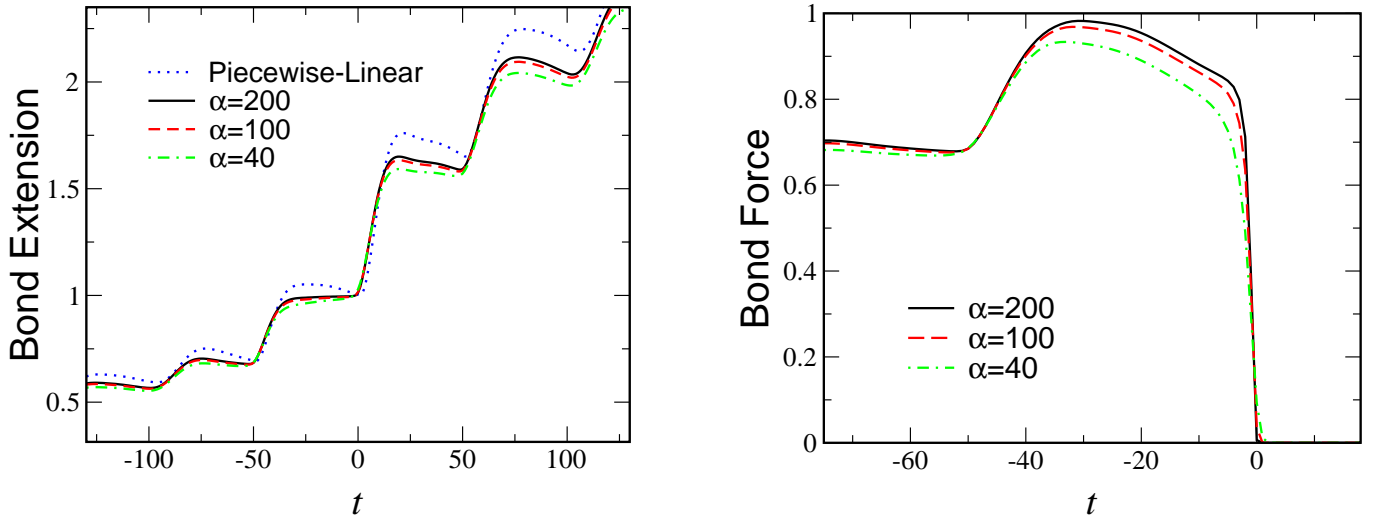


FIG. 3: a) Bond extension along crack surface versus  $t$ , for  $\alpha = 40, 100$  and  $200$  together with the piecewise-linear model results. b) Bond force along crack surface versus  $t$ , for  $\alpha = 40, 100$  and  $200$ . In both figures,  $N = 3$ ,  $\eta = 0.25$ ,  $v = 0.1$  and  $dt = .1$ .

model. We see that for velocities less than about  $0.6c$ , the curves basically coincide, with the smallest  $\alpha$  curve lying slightly below the others. However, in the range  $0.6c < v < 0.7c$ , the data exhibit a marked sensitivity to  $\alpha$ . The low  $\alpha$  curve is flat in this region, and as  $\alpha$  is increased, monotonicity is destroyed and a local maximum and minimum are created. These features are completely absent in the piecewise-linear data, indicating that the additional bond breaking, absent by construction in the piecewise-linear solution, is responsible. Clearly, once a local maximum in  $v$  versus  $\Delta$  sets in, as it does for large enough  $\alpha$ , the steady-state solutions are unstable for  $\Delta$ 's past the maximum. We address this issue in the next section, where we perform a stability analysis of the steady-state solutions. Nevertheless, it is interesting to note that past this band of velocities, the dependence on  $\alpha$  is again very mild, but very different from the piecewise-linear results.

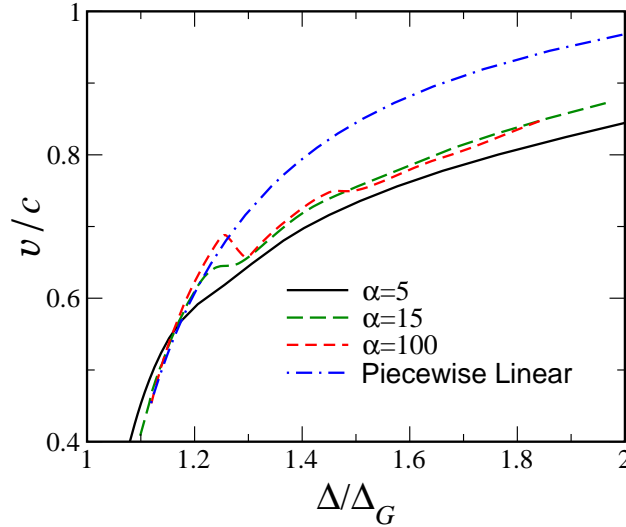


FIG. 4:  $v/c$  versus  $\Delta/\Delta_G$  for  $N = 8$ ,  $\eta = 0.1$ . Data is presented for the cases  $\alpha=5, 15$ , and  $100$ , and well as for the piecewise-linear model.

## V. STABILITY ANALYSIS

Next, we consider the linear stability of the traveling wave state given by the aforementioned Slepian ansatz  $u_{x,y}(t) = u_y(t - v/x)$ . Specifically, we assume a solution of the form

$$u_{x,y}(t) = u_y^{(0)}(\tau) + e^{-\omega x} \delta u_y(\tau) \quad (5)$$

where  $\tau$  is the traveling wave coordinate  $t - x/v$  and  $u^{(0)}$  is the previously determined solution. For the stability problem, we take  $\delta u \ll 1$  and expand to linear order. Note that the last term can be written in the alternate form  $e^{\omega v t} \tilde{\delta u}_y(\tau)$  with

$$\tilde{\delta u}_y(\tau) = \delta u_y(\tau) e^{v\omega\tau} \quad (6)$$

Hence, for stability we must have  $\text{Re } \omega < 0$ , i.e. perturbations must decay in time at a fixed position in the frame moving with the crack tip.

We substitute this assumption into the equation of motion. This leads to the linear problem

$$\begin{aligned} \frac{d^2}{d\tau^2} \delta u_y(\tau) = & \sum_{nn} G(\vec{x}, \vec{x}') \left( \delta u_y(\tau) - \delta u_{y'}(\tau') e^{\omega(x-x')} \right) \\ & + \eta k_{\vec{x}, \vec{x}'} \left( u_y^{(0)}(\tau) - u_{y'}^{(0)}(\tau') \right) \frac{d}{d\tau} \left( \delta u_y(\tau) - \delta u_{y'}(\tau') e^{\omega(x-x')} \right) \end{aligned} \quad (7)$$

where we have defined

$$G(\vec{x}, \vec{x}') = f' \left( u_y^{(0)}(\tau) - u_{y'}^{(0)}(\tau') \right) + \eta k'_{\vec{x}, \vec{x}'} \left( u_y^{(0)}(\tau) - u_{y'}^{(0)}(\tau') \right) \frac{d}{d\tau} \left( u_y^{(0)}(\tau) - u_{y'}^{(0)}(\tau') \right) \quad (8)$$

and of course  $\tau' = t - x'/v$ .

To find the allowed values of  $\omega$ , we proceed as follows. First, we impose the asymptotic boundary conditions that at all  $\vec{x}$  outside of our explicit lattice points,  $\delta u = 0$ . We then pick an arbitrary normalization by fixing  $\delta u_{y=\sqrt{3}/4}(0) = 1$  and simultaneously relax the equation of motion at that same point. This procedure, implemented for some guessed value of  $\omega$ , converts our problem into an inhomogeneous, banded system of linear equations for the complex variables  $\delta u_y(\tau)$  which can be solved by standard techniques. The missing equation then forms a complex mismatch function whose zeroes then determine the allowed values of the eigenvalue  $\omega$ .

Two other details should be noted. First, we do not impose any symmetry restrictions on our perturbation with respect to reflections about the crack plane. Also, any time we find a root with some specific value of  $\text{Im } \omega$ , an equivalent solution exists with

$$\begin{aligned} \text{Im } \omega & \rightarrow 2\pi - \text{Im } \omega \\ \delta u_y & \rightarrow \delta u_y^* \quad (\text{even rows}) \\ \delta u_y & \rightarrow -\delta u_y^* \quad (\text{odd rows}) \end{aligned} \quad (9)$$

By even and odd, we mean the parity of the lattice units of distance from the row  $y = \sqrt{3}/4$ . This result follows from the fact that the governing equation is real and that the  $x$  spacing of nearest neighbor points on the rows separated by an even number is  $\pm 1$ , whereas it is  $\pm \frac{1}{2}$  for odd rows. A corollary of this is that a root at exactly  $\text{Im } \omega = \pi$  has an eigenfunction which is purely real on even rows and purely imaginary on odd ones.

One obvious test of our stability analysis arises from the fact that translation invariance guarantees that there is a root at  $\omega = 0$  with eigenfunction

$$\delta u_y(\tau) = \frac{d}{d\tau} u_y^{(0)}(\tau) / \frac{d}{d\tau} u_{y=\sqrt{3}/4}^{(0)}(0) \quad (10)$$

Actually, our discretization for numerical purposes of the continuous variable  $\tau$  breaks this exact invariance and hence the mode should be at zero only in the small  $d\tau$  limit. In the data we present below, the zero mode is found with a typical accuracy of  $10^{-2}$ , and the eigenfunction to the same accuracy agrees with its expected form.

In Fig. 5a, we show the basic result that emerges from our analysis, namely that as the driving displacement is increased, there is a mode which crosses the stability threshold. In Fig. 5b, we show the associated  $\text{Im } \omega$ . At the point of instability,  $\text{Im } \omega$  is close to but not exactly equal to  $\pi$ . Were it equal to  $\pi$ , this would be a period-doubling instability, as the perturbative displacements at neighboring  $x$  values (at the same  $\tau$ ) would alternate in sign. More

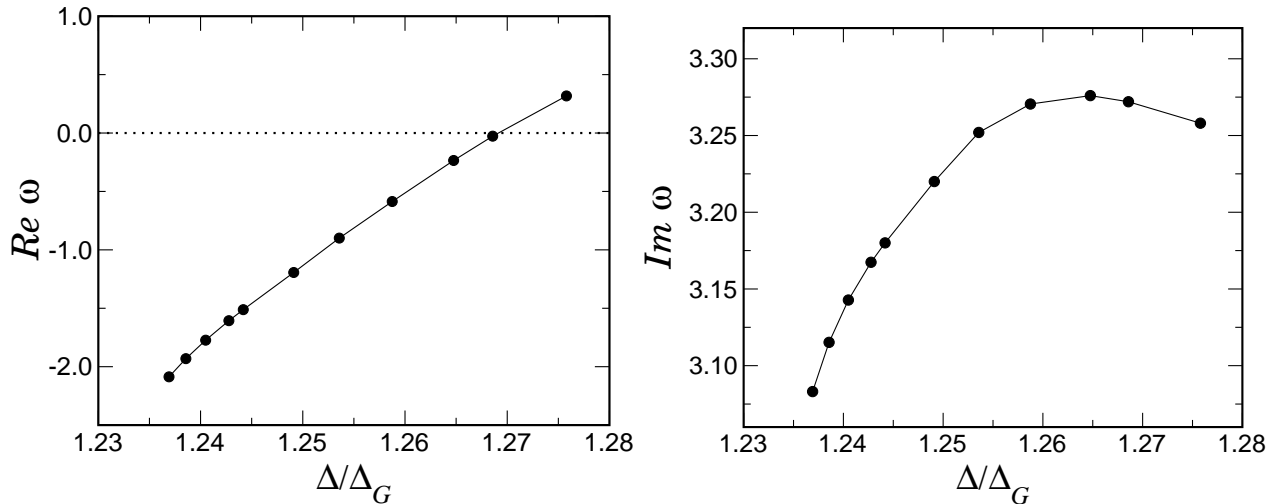


FIG. 5: Eigenvalue for stability problem, with  $N=8$ ,  $\alpha = 15$  and  $\eta = .1$ . The calculation was done with  $L = 200$  and  $n_b=12$ ; note that by definition  $v = 1/(n_b dt)$ .  $Re \omega$  is shown in (a),  $Im \omega$  in (b).

general values of  $Im \omega$  signify a Hopf bifurcation which in general has a frequency incommensurate with the original frequency associated with moving one lattice spacing. The signature of such a bifurcation should be a slowly oscillating crack tip speed, with the oscillation frequency  $\omega_{tip} = |Im \omega - \pi|$ .

In Fig. 6, we show the real part of the eigenfunction for the rows  $y = \pm\sqrt{3}/4$  as a function of the traveling wave coordinate  $\tau$ . Note that the perturbation is almost, but not exactly, antisymmetric around the crack plane. The eigenvector decays slowly downstream and very rapidly upstream of the crack tip; it is therefore a localized mode connected with the tip dynamics diverging from the pure Slepyan form.

In previous studies of piecewise-linear models (which correspond to the limit  $\alpha \rightarrow \infty$ ), it was noted that the Slepyan solution breaks down above a critical velocity. There, the criterion for this breakdown was connected to the fact that certain bond extensions other than those along the presumed crack line go above the breaking threshold. In our current model where the force-law is analytic, there is no such criterion and the steady-state solution found by our procedure does not need to be checked for any auxiliary condition. On the other hand, we do observe a linear instability. It is therefore of interest to compare these two criteria, i.e. to investigate whether the stability criterion in the large  $\alpha$  limit goes over smoothly to the inconsistency criterion for the ideally brittle case. To do this, we have plotted in Fig. 7 the horizontal bond extension along the crack line for a steady-state solution at  $\alpha = 50$  right at the onset of the linear instability. Note that the bond extension is extremely close (roughly of order  $1/\alpha$ ) to what would be the breaking threshold. Thus, the results of the ideally brittle case as to where nontrivial spatio-temporal dynamics of the crack tip sets in are not an artifact of the force-law discontinuity; i.e., smoothing the spring law does not alter the basic conclusion. This is good news, as the ideal case has proven rather amenable to analytic techniques which enable calculations to be done for much larger  $N$  (even for infinite  $N$ ) than is possible for any direct numerical scheme.

One nagging question posed by our results concerns the fact that the instability is so close to but not exactly at the period-doubling point of  $Im \omega = \pi$ . We have investigated whether there is any tendency for the mode to get pinned at the period-doubling point as parameters are varied, as certain limits are reached etc.. For example, in Fig. 8 we show  $Im \omega$  at threshold versus  $\alpha$ . As far as we have been able to determine, this pinning does not occur and the generic bifurcation always leads to an incommensurate oscillating tip state. We will compare this prediction with direct numerical simulations of the equations of motion in the next section.

## VI. COMPARISON TO SIMULATION

In order to test the results of the stability analysis, and also to investigate the nature of the dynamics past the instability threshold, we have implemented a direct numerical simulation of the equations of motion. Our system is a triangular lattice, of width  $2N + 2$  whose top and bottom rows are fixed to have displacement  $\pm\Delta$ . We start with a uniformly strained state, except for the first few left hand columns of mass points. The initial displacement of these points is taken to vary linearly in  $x$  from  $\pm\Delta$  at  $x = 0$  to the that of the uniformly strained state at  $x = 10$ . The equations of motion are then stepped forward in time, using a simple Euler scheme. We track the velocity of the crack

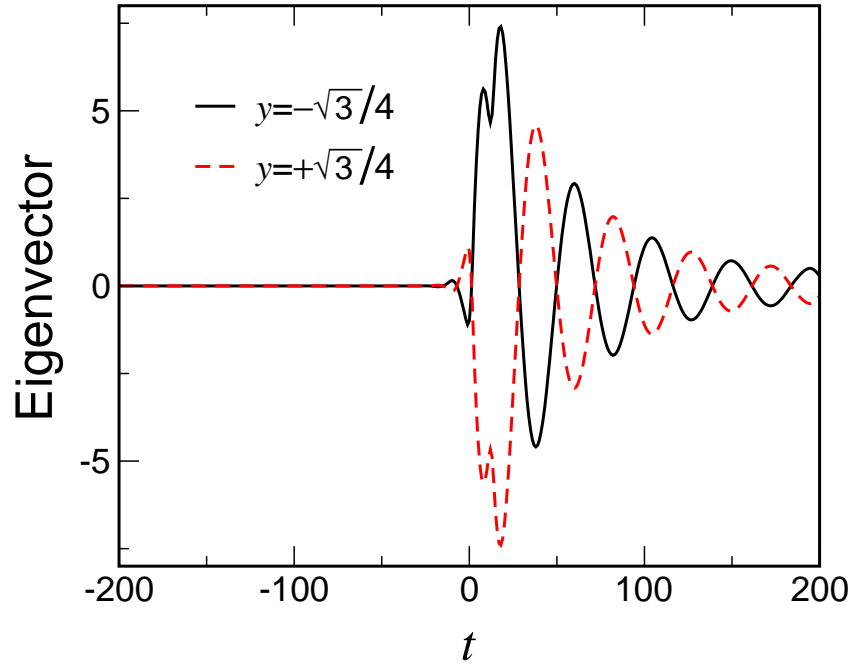


FIG. 6: Eigenvector for stability problem, with  $N=4$ ,  $\alpha = 50$  and  $\eta = .2$ . The calculation was done with  $L = 200$  and  $n_b=12$ , and at the point of instability,  $dt = .08702$ .

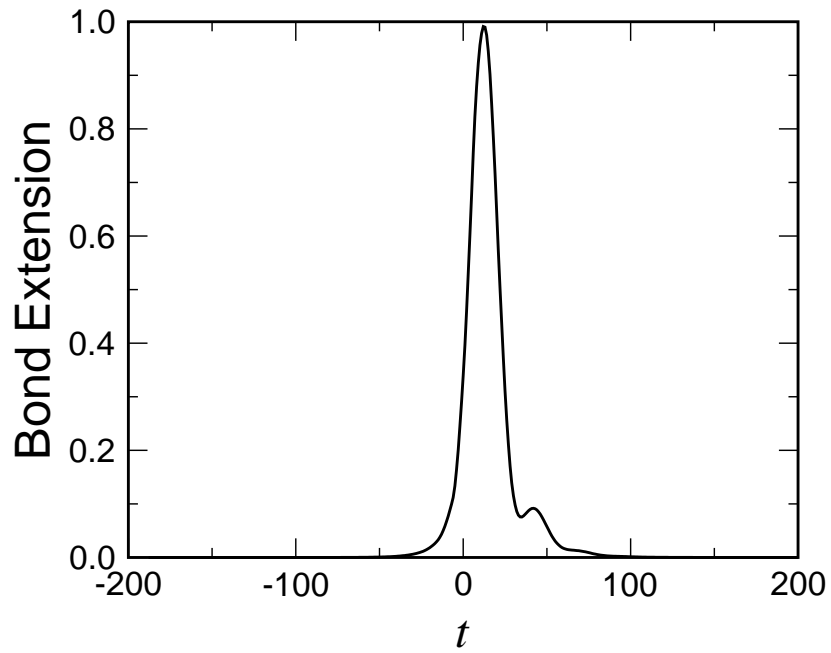


FIG. 7: Horizontal bond extension for marginally stable solution, with  $N=4$ ,  $\alpha = 50$  and  $\eta = .2$ . The calculation was done with  $L = 200$ ,  $nb = 12$ , and  $dt = .08702$ .



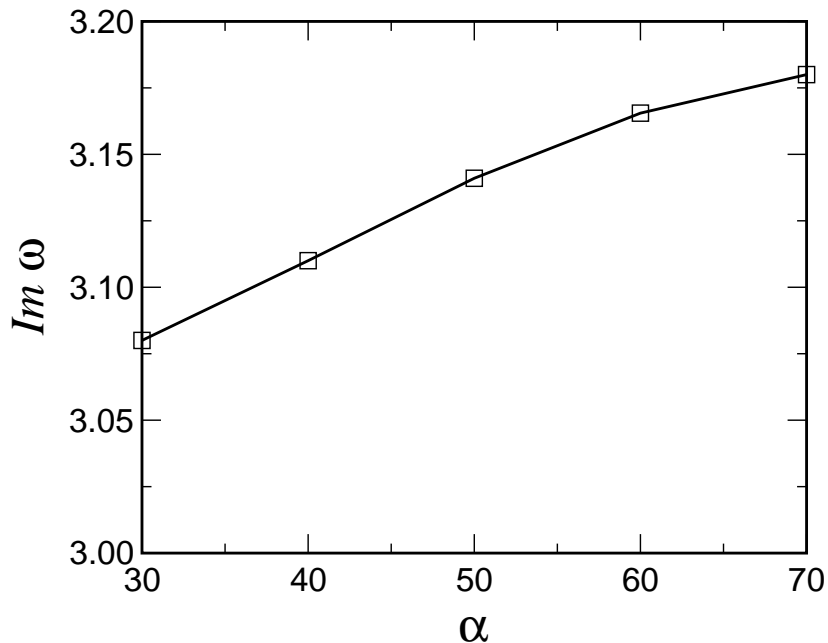


FIG. 8: Variation of  $\text{Im } \omega$  at the marginal stability point with  $\alpha$ ; data is all for  $N=4$ ,  $\eta = .2$ .

by monitoring the bond extensions, and noting when they exceed unity, which we take as our criterion of cracking. Note that in this model, cracking is in principle a reversible process and so this criterion is merely a convenient way of keeping track of the dynamics and not an intrinsically important threshold.

As expected, for moderate  $\Delta$  the only bonds that “crack” are the diagonal bonds that span the midline. The time between cracking events is constant, and, to best compare with our steady-state calculations above, we fix our time step  $dt$  in each case so that there are 6 time steps between each cracking event; this can then be directly compared to our steady-state solutions computed with time bandwidth  $n_b \equiv 1/(v dt) = 12$ . We find that the velocities obtained in this way reproduce extremely well the velocities calculated by our steady-state code.

As we increase  $\Delta$  above the critical value for instability calculated in the previous section, we indeed find that the pattern of steady-state cracking breaks down. Some horizontal bonds on the crack surface begin to crack, and the average velocity of the crack falls dramatically, presumably due to the draining of energy by these extra cracking events. It is important to note that these broken horizontal bonds are always *behind* the crack tip, in accord with the calculations of the piecewise-linear model. It is not clear whether there is in fact a discontinuous drop in the average velocity. The shape of the drop does appear to be insensitive to the  $dt$  chosen, so that it in any event does not appear to be a numerical artifact of finite  $dt$ .

As a test of our stability calculation, we have computed the Hopf frequency directly from the numerical simulation. We fixed  $\Delta$  to lie slightly higher than the critical value for the onset of the instability and measured, at the moment of the breaking of a northeast- southwest diagonal bond, the extension of the bond. Due to the discreteness of the time step, this is somewhat larger than unity. If we had true steady-state propagation, this value would be constant. Instead, for this  $\Delta$ , we find that the value oscillates about some value, with the magnitude of the oscillation growing in time. The growth we associate with the small positive growth rate of the perturbation in the unstable state, and the frequency of oscillation with the Hopf frequency. In Fig. 9, we show the data. The period of oscillation is essentially 1, (in other words, the time between breakings of this type of bond), which corresponds to a Hopf frequency of essentially  $\pi$ . By numerically fitting a sine wave to the data, we find that the Hopf frequency is approximately 3.272, in very good agreement with the stability calculation result shown in Fig. 5b.

As we increase  $\Delta$  further, at some point the average velocity starts to increase again. Examining the solution in this region in more detail, we show in Fig. 10 the time history of three adjacent points on the crack surface. We see that the third trace is identical to the first, and differs significantly from the second. It appears then that the system has settled into a new kind of steady-state solution, more complex than the simple Slepian form. To test this, we implemented a new steady-state algorithm, designed to allow for this period-2 type solution. We assumed that in each row there are two possible time histories for particles, which alternate. We also did not assume any symmetry across the crack surface. Taking care to organize the storage so that the banded structure is maintained, we employed our banded Newton’s method. Working for the sake of computational convenience at  $N = 4$ , the algorithm succeeded in

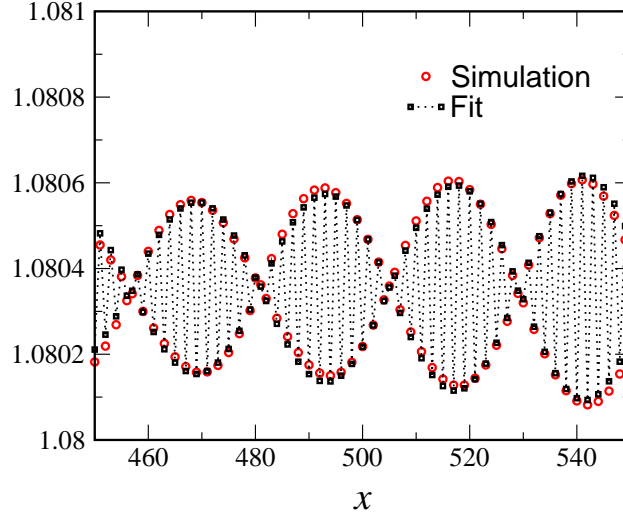


FIG. 9: Bond extension at breaking as a function of position  $x$  along the crack surface. Here  $N = 8$ ,  $\eta = .1$ ,  $\alpha = 15$ ,  $\Delta = 2.6215$ ,  $\Delta/\Delta_G = 1.2693$ ,  $dt = 0.1053852$ . The fitted curve is  $3.57 \cdot 10^{-5} \sin(3.27166x - 2.85642) \exp(0.00368x)$ .

obtaining steady-state solutions where the symmetry between the two time histories (as well as up-down symmetry across the crack surface) is broken. We traced out the velocity- $\Delta$  relation for this solution. We find that the line of solutions is disconnected from the symmetric branch and that in general there are multiple solutions for each  $\Delta$ . Starting from a solution obtained from using the simulation to obtain an initial guess, we tracked the solution as we varied  $\Delta$ . The velocity decreased with decreasing  $\Delta$  and then turned around and after some wandering headed off to large  $\Delta$  with the velocity higher than the original branch. Thus it is the *slower* branch which is physically realized. This data is presented in Fig. 11, along with the (time-averaged) velocities measured in simulation.

It is reasonable to assume that the existence of a period-doubled solution very close to the original symmetric branch is associated with the fact that the Hopf bifurcation is nearly period-doubling. To check this notion, we note that it was found in the previous section that the Hopf-frequency passed through  $\pi$  for some particular value of  $\alpha$ . For this value, one expects the period-doubled branch to hit the main branch, corresponding to a higher co-dimension bifurcation. To address this question, we have also traced out the bifurcated solution for  $\alpha = 40$ , which is very slightly below this crossing point. The amazingly baroque solution curve is presented in Fig. 12, together with the symmetric branch. We see that the bifurcated solution curve turns up to approach the symmetric curve, before veering away. Examination of the solutions indicate that the asymmetry is extremely small in this region of close

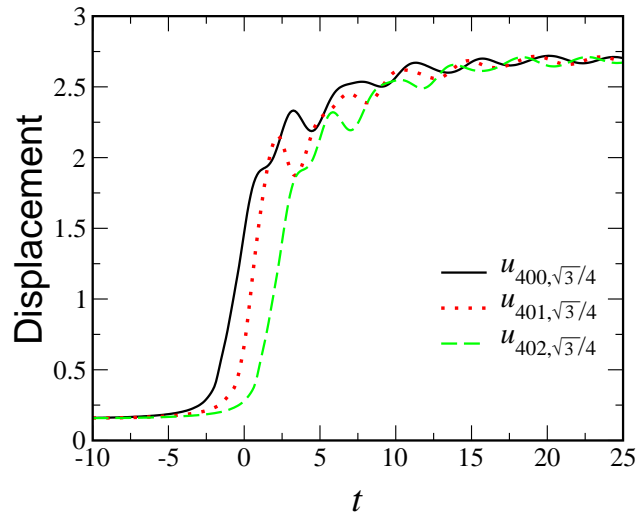


FIG. 10: Time trace of displacement of three adjacent points on the upper crack surface. Here  $N = 8$ ,  $\eta = .1$ ,  $\alpha = 15$ ,  $\Delta = 2.7$ ,  $\Delta/\Delta_G = 1.3073$ ,  $dt = 0.10858$ .

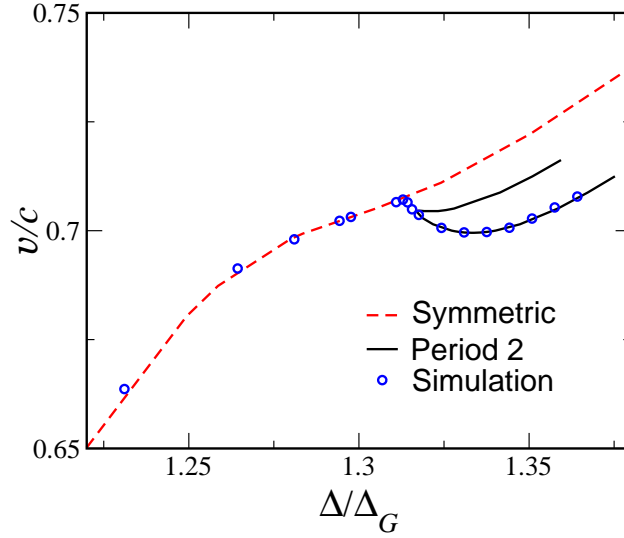


FIG. 11: Velocity vs.  $\Delta/\Delta_G$  for symmetric and period-2 solutions, together with measured (time-averaged) velocity from simulation.  $N = 4$ ,  $\eta = 0.1$ ,  $\alpha = 15$ .

approach. Presumably, then, at the crossing value of  $\alpha$  the bifurcated solution actually meets the symmetric branch, and the bifurcation is perfect at this point. As the meeting is not on the presumably stable branch of the bifurcated solution, the bifurcation should prove to be subcritical. A detailed study of the nature of the bifurcation should prove mathematically interesting, though not necessarily physically relevant. It should be noted that we have also uncovered another, apparently disconnected, branch of period-2 solutions. These other solutions presumably play an important role in the exact nature of the bifurcation, though again they do not seem to be important for the physics.

Increasing  $\Delta$  further, the simulation tracks the bifurcated steady-state solution until at some point yet additional bonds are broken, and the velocity falls below that of the bifurcated solution. The time-dependence of this state becomes more complicated than the simple period-2 structure of the bifurcated steady-state. It is important to point out that the additional bonds are also always located behind the crack tip, which remains on the midline. Thus the additional bond breaking is reminiscent of side-branching in dendritic growth [16]; i.e., a phenomenon induced by the tip and which is left behind by the growing crack. As opposed to dendritic growth, in Mode III fracture the sidebranching is generated intrinsically by the tip, and is not noise-induced [17]. We see, however, no tendency for the tip itself to leave the midline. This can be seen in Fig. 13, where the broken bonds are portrayed for two different values of  $\Delta$ . Also, the picture shows that as the driving is increased the size of the sidebranches increases, but they

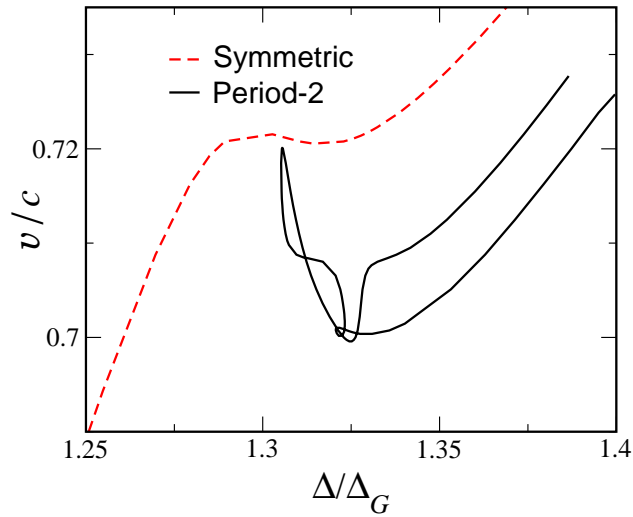


FIG. 12: Velocity vs.  $\Delta/\Delta_G$  for symmetric and period-2 solutions.  $N = 4$ ,  $\eta = 0.1$ ,  $\alpha = 40$ .

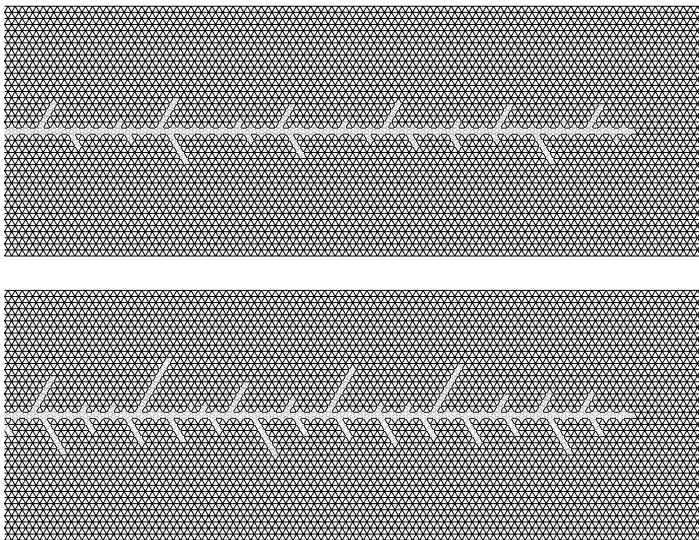


FIG. 13: Broken bonds for  $N = 20$ ,  $\eta = .1$ ,  $\alpha = 15$ . (Top)  $\Delta=5.5$ ,  $\Delta/\Delta_G=1.715$ ; (Bottom)  $\Delta=6.5$ ,  $\Delta/\Delta_G=2.207$

are always microscopic, growing to a length of about 8 at the larger  $\Delta$ . In this latter picture, the crack is moving at an average velocity of  $v/c = .789$ , which is quite fast. Furthermore, the sidebranches are not only short, but the sidebranching period is also on the lattice scale. Thus, the claim of [11] that these sidebranches are related to the experimentally seen micro-branching appears to us doubtful, especially in light of our preliminary work on Mode I cracking [18], where the tip dynamics is very different. This issue is worthy of further exploration.

### Acknowledgments

The work of DAK is supported in part by the Israel Science Foundation. DAK thanks the Lawrence Berkeley National Laboratory, where this work was initiated, for its hospitality. HL is supported in part by the US NSF under grant DMR98-5735.

## VII. APPENDIX - SOLVING THE ALMOST BANDED PROBLEM

In this appendix, we outline how to efficiently solve the linear problem associated with the Newton's method treatment of the nonlinear steady-state problem. It is important to set up the problem correctly to achieve an almost-banded structure. We order the variables with the  $y$  index running more quickly, since we want  $N \ll 2L + 1$ , the length of the system in the  $x$  direction. We order the equations similarly, replacing the equation of motion for the site  $x = 0$ ,  $y = \sqrt{3}/4$  (where  $x$  runs from  $-L$  to  $L$ ) by the constraint equation  $u = u_0$ , where the constant  $u_0$  can be chosen arbitrarily. The equation of motion for the site  $(0, \sqrt{3}/4)$  is taken to be the last equation. We also note that equations of motion have to be taken for the columns  $-L - 1 \leq x \leq L - 1$ , since the number of linear modes which diverge as  $x \rightarrow -\infty$  is one greater than the number which diverge for large positive  $x$  (see [6, 7]) due to the presence of the third derivative operator.

The problem then has the structure

$$\begin{pmatrix} \mathcal{M}_b & V \\ W^T & 0 \end{pmatrix} \begin{pmatrix} \delta U \\ \delta \Delta \end{pmatrix} = \begin{pmatrix} A \\ b \end{pmatrix} \quad (11)$$

Here,  $\mathcal{M}_b$  is a banded square matrix of size  $N(2L+1)$  with lower bandwidth  $N(n_b+2)$  and upper bandwidth  $N(n_b+1)$  (with  $n_b$  an integer such that the velocity is  $v = 1/(n_b dt)$ ). The replacement of the equation for the distinguished site  $(0, \sqrt{3}/4)$  is necessary to ensure that  $\mathcal{M}$  is not singular. The length  $N(2L+1)$  vector  $V$  contains the derivatives of the equations of motion with respect to  $\Delta$  and the vector  $W$  contains the equation of motion for the distinguished site (which does not depend on  $\Delta$ ). The shift in the displacements  $\delta U$ , and the source  $A$  are also vectors of length

$N(2L+1)$ , and  $\delta\Delta$  and  $b$  are numbers. We can explicitly solve this system in terms of  $\mathcal{M}_b^{-1}$ , which is easy to compute due to its banded structure. We find

$$\begin{aligned}\delta\Delta &= \frac{W^T \mathcal{M}_b^{-1} A - b}{W^T \mathcal{M}_b^{-1} V} \\ \delta U &= \mathcal{M}_b^{-1} (A - (\delta\Delta)V)\end{aligned}\tag{12}$$

Hence, our entire system can be solved with no more effort than would be required for a fully banded problem.

- 
- [1] For a review, see J. Fineberg and M. Marder, Phys. Repts. **313**, 2 (1999).
  - [2] J. Fineberg, S. P. Gross, M. Marder and H. L. Swinney, Phys. Rev. Lett. **67**, 457 (1992); Phys. Rev. B **45**, 5146 (1992); E. Sharon, S. P. Gross and J. Fineberg, Phys. Rev. Lett. **74**, 5096 (1995); Phys. Rev. Lett. **76**, 2117 (1996).
  - [3] L. I. Slepyan, Doklady Akademii Nauk SSSR **258**, 561 (1981) [Sov. Phys. Dokl. **26**, 538 (1981)].
  - [4] S. J. Zhou, D. M. Beazley, P.S. Lomdahl, and B. L. Holian, Phys. Rev. Lett. **78**, 479 (1997) ; P. Gumbsch, S. J. Zhou, and B. L. Holian, Phys. Rev. B **55**, 3445 (1997); D. Holland and M. Marder, Phys. Rev. Lett. **80**, 746 (1997).
  - [5] M. Marder and S. Gross, J. Mech. Phys. Solids **43**, 1 (1995).
  - [6] D. A. Kessler and H. Levine, Phys. Rev. E **59**, 5154 (1998).
  - [7] D. A. Kessler, Phys. Rev. E **61**, 2348 (2000).
  - [8] L. Pechenik, H. Levine and D. A. Kessler, “Exact solution for steady-state mode III cracks in a viscoelastic lattice model”, preprint (1999); “Steady-state mode I cracks in a viscoelastic triangular lattice”, preprint (1999).
  - [9] D. A. Kessler and H. Levine, Phys. Rev. E **60**, 7569 (1999).
  - [10] Sh. A. Kulamekhtova, V. A. Saraikin and L. I. Slepyan, Mech. Solids **19**, 102 (1984).
  - [11] M. Marder and X. Liu, Phys. Rev. Lett. **71**, 2417 (1993).
  - [12] J. S. Langer, Phys. Rev. A **46**, 3123 (1992).
  - [13] J. A. Hauch, D. Holland, M. P. Marder, and H. L. Swinney, Phys. Rev. Lett. **82**, 3823 (1999).
  - [14] A. Paskin, D. K. Som, and G. J. Dienes, Acta Metallurgica **31**, 1841 (1983).
  - [15] O. Pla, F. Guinea, E. Louis, S. V. Ghasias and L. M. Sander, Phys. Rev. B **57**, R13981 (1998).
  - [16] D. A. Kessler, J. Koplik and H. Levine, *Adv. Phys.* **37**, 255-339 (1988).
  - [17] E. Brener and D. Temkin, Phys. Rev. E **51**, 351 (1995).
  - [18] D. A. Kessler and H. Levine, in preparation.